Tunable 1D van der Waals Nanostructures by Vapor-Liquid-Solid Growth

Peter Sutter[1,*] and Eli Sutter[2,3,*]

[1]Department of Electrical & Computer Engineering, University of Nebraska-Lincoln, Lincoln, NE 68588

[2]Department of Mechanical & Materials Engineering, University of Nebraska-Lincoln, Lincoln, NE 68588

[3]Nebraska Center for Materials and Nanoscience, University of Nebraska-Lincoln, Lincoln, NE 68588

*Corresponding authors, e-mail: psutter@unl.edu, esutter@unl.edu.

CONSPECTUS

Vapor-liquid-solid (VLS) growth using molten metal catalysts has traditionally been used to synthesize nanowires from different 3D-crystalline semiconductors. With their anisotropic structure and properties, 2D/layered semiconductors create additional opportunities for materials design when shaped into 1D nanostructures. In contrast to hexagonal 2D crystals such as graphene, h-BN, and transition metal dichalcogenides, which tend to roll up into nanotubes, VLS growth of layered group III and group IV monochalcogenides produces diverse nanowire and nanoribbon morphologies that crystallize in a bulk-like layered structure with nanometer-scale footprint and lengths exceeding tens of micrometers. In this Account, we discuss the achievable morphologies, the mechanisms governing key structural features, and the emerging functional properties of these 1D van der Waals (vdW) architectures. Recent results highlight rich sets of phenomena that qualify these materials as a distinct class of nanostructures, far beyond a mere extension of 3D-crystalline VLS nanowires to vdW crystals.

The main difference between 3D- and vdW crystals, the pronounced in-plane/cross-plane anisotropy of layered materials, motivates investigating the factors governing the layer orientation. Recent research suggests that the VLS catalyst plays a key role, and that its modification *via* the choice of chalcogens or through modifiers added to the growth precursor can switch both the nanostructure morphology and vdW layering. In many instances, ordinary

layered structures are not formed but VLS growth is dominated by morphologies – often containing a crystal defect – that present reduced or vanishing layer nucleation barriers, thus achieving fast growth and emerging as the principal synthesis product. Prominent defect morphologies include vdW bicrystals growing by a twin-plane reentrant process and chiral nanowires formed by spiral growth around an axial screw dislocation. The latter carry particular promise, *e.g.*, for twistronics. In vdW nanowires, Eshelby twist – a progressive crystal rotation caused by the dislocation stress field – translates into interlayer twist that is precisely tunable *via* the wire diameter. Projected onto a helicoid vdW interface, the resulting twist moirés not only modify the electronic structure but also realize configurations without equivalent in planar systems, such as continuously variable twist and twist homojunctions.

1D vdW nanostructures derive distinct functionality from both their layered structure and embedded defects. Correlated electron microscopy methods including imaging, nanobeam diffraction, as well as electron-stimulated local absorption and luminescence spectroscopies combine to an exceptionally powerful probe of this emerging functionality, identifying twist-moiré induced electronic modulations and chiral photonic modes, demonstrating the benign nature of defects in optoelectronics, and uncovering ferroelectricity *via* symmetry-breaking by single-layer stacking faults in vdW nanowires. Far-reaching possibilities for tuning crystal structure, morphology, and defects create a rich playground for the discovery of new functional nanomaterials based on vdW crystals. Given the prominence of defects and extensive prospects for controlling their character and placement during synthesis, 1D vdW nanostructures have the potential to cause a paradigm shift in the science of electronic materials, replacing the traditional strategy of suppressing crystal imperfections with an alternative philosophy that embraces the use of individual defects with designed properties as drivers of technology.

KEY REFERENCES

- Sutter, P.; Wimer, S.; Sutter, E., Chiral twisted van der Waals nanowires, *Nature* **2019**, 570, 354-357.[1] *This work introduced van der Waals nanowires for twistronics. GeS nanowires predominantly form as growth spirals around an axial screw dislocation that causes Eshelby twist. This produces a precision small-angle twist moiré modulating the electronic structure along the nanowires.*

- Sutter, E.; French, J.S.; Sutter, P., Tunable layer orientation and morphology in vapor-liquid-solid growth of one-dimensional GeS van der Waals nanostructures, Chemistry of Materials **2021**, 33, 3980-3988.[2] *This paper established that growth modifiers switch morphology and layer orientation of GeS van der Waals nanostructures. The results demonstrated layering between that of nanowires and nanoribbons and showed that the layer orientation can be controlled via the growth catalyst.*

- Sutter, E.; French, J.S.; Komsa, H.-P.; Sutter, P., 1D Germanium sulfide van der Waals bicrystals by vapor–liquid–solid growth, *ACS Nano* **2022**, 16, 3735-3743.[3] *This paper introduced twinned van der Waals bicrystals as a fast-growing VLS nanostructure. Nanometer-scale cathodoluminescence spectroscopy quantified the effects of defects on radiative recombination, demonstrating that the twin defect enabling fast growth has no negative impact on the optoelectronic properties.*

- Sutter, E.; Komsa, H.-P.; Puretzky, A.A.; Unocic, R.R.; Sutter, P., Stacking fault induced symmetry breaking in van der Waals nanowires, *ACS Nano* **2022**, 16, 21199-21207.[4] *This work introduced symmetry breaking by single-layer stacking faults in van der Waals nanowires as a mechanism for generating ferroelectricity in crystals with otherwise centrosymmetric equilibrium layer stacking.*

1. INTRODUCTION

The emergence of atomically thin (2D) crystals[5,6] provides motivation to harness the extraordinary properties of 2D or layered van der Waals (vdW) materials by incorporating them in one-dimensional (1D) nanostructures, thereby enriching them with confinement effects, a large surface to volume ratio, low-dimensional charge- and spin transport, and unusual optical and photonic properties. Indeed, 1D structures of sp^2-bonded carbon,[7] h-BN,[8] WS_2,[9] and MoS_2[10] have been explored in the form of nanotubes significantly before the advent of planar monolayers of the same materials, aided by the strong propensity of such hexagonal or trigonal 2D/layered crystals for forming cylindrical tubes consisting of single or multiple nested sheets.

In this Account, we discuss 1D nanostructures of other classes of 2D/layered crystals, notably monochalcogenides of group III (Ga) and group IV elements (Ge, Sn) as well as their alloys, which set themselves apart (from nanotubes, vdW solids consisting of 1D chains,[11] *etc*.) by forming 1D (wire-like) nanostructures in metal catalyzed vapor-liquid-solid (VLS)[12] processes while crystallizing in their bulk layered structure, *i.e.*, with essentially planar layers.[13] At first glance, this may appear as a straightforward extension of the well-known concept of VLS growth of 3D-crystalline semiconductor nanowires to van der Waals crystals. However, research during the past few years found surprisingly rich phenomena for 1D vdW nanostructures in synthesis, structure, and emergent properties. They include distinct synthesis challenges, *e.g.*, obtaining control over the layer orientation; behaviors such as the evolutionary selection of prominent fast-growing defect morphologies in VLS processes; exotic structures including precision small-angle twist moirés projected onto helicoid vdW interfaces; and emerging functional properties of interest for twistronics, optoelectronics, photonics, ferroelectrics, *etc.*, which often do not arise *in spite of* defects but *because* of them. While there have been isolated

early reports of 1D nanostructures of different vdW crystals, including GaSe,[14] GeSe,[15] In_2Se_3,[16] and Sb_2Se_3,[17] the systematic exploration of synthesis, structure, morphology, and functionality in VLS-grown vdW architectures began relatively recently and the young field promises abundant opportunities for fundamental insight, technological developments, as well as surprise discoveries for years to come.

2. CONTROL OVER THE LAYER ORIENTATION

One of the main differences between 3D-crystalline semiconductors (*e.g.*, Si, Ge, GaAs) and vdW semiconductors lies in the anisotropic chemical bonding of layered crystals – covalent intralayer bonding combined with weak dispersive interlayer forces – compared to the 3D periodicity and bonding of conventional crystals. From this structural anisotropy follow anisotropic properties, as illustrated by the classic example of graphite where large differences exist between in-plane and out-of-plane electrical conductivity,[18] thermal conductivity,[19] magnetic susceptibility,[20] *etc*. 1D nanomaterials offer special opportunities for harnessing these anisotropies in applications, provided that mechanisms can be identified for controlling the layer orientation during synthesis. The two limiting cases – nanowires and nanoribbons with layer stacking parallel and perpendicular to the growth direction, respectively – are illustrated in Figure 1 (a)–(b). Between these limits, it may be of interest to tune to any desired layer orientation, but tailoring VLS growth to achieve such continuously variable layering is extremely challenging.

The feasibility of changing the lattice orientation in nanowires was demonstrated for 3D-crystalline semiconductors, *e.g.*, in Au-catalyzed VLS synthesis of Si nanowires where reducing the wire diameter changes the growth direction from <111> to <110>.[21,22] Recent work provided evidence for the crucial role of the VLS catalyst in determining the layer orientation during the

growth of vdW nanostructures. In VLS growth of the layered semiconductor gallium(II) sulfide (GaS), for example, different morphologies are obtained with Au and Ag catalysts.[23] Growth over Au catalyst yields GaS nanoribbons with a characteristic zigzag morphology and decreasing width toward the tip. Growth over Ag catalysts, on the other hand, produces both tapered nanowires and long (up to 100 μm) nanoribbons with uniform width. The example of another Ga monochalcogenide, GaSe, indicates that a mere change of the chalcogen species can tip the balance between these two morphologies toward pure nanoribbons, which are ultrathin, uniform in width (matching the catalyst size), and terminated by exceptionally smooth edges and top/bottom facets.[24]

Additional insight into the factors controlling the layer orientation was obtained for Au-catalyzed VLS growth of nanostructures of the monochalcogenides GeS and GeSe as well as $GeS_{1-x}Se_x$ alloys (Figure 1 (c)–(e)). We note that VLS growth of these materials predominantly selects fast-growing defect morphologies, which we discuss in more detail in Section 3. Within the $GeS_{1-x}Se_x$ system, both nanowires and nanoribbons can be accessed under similar growth conditions by adjusting the precursor composition. Materials from pure GeS to selenium-rich $GeS_{0.08}Se_{0.92}$ alloys crystallize as nanowires (Figure 1 (c)),[1,4] albeit in different forms, namely growth spirals around an axial screw dislocation for S-rich GeS_xSe_{1-x} alloys ($0.6 \leq x \leq 1$) and layered wires with *c*-axis parallel to the growth direction for $x < 0.6$.[4] Close to pure GeSe, the morphology switches to large, ultrathin van der Waals ribbons where simultaneous longitudinal VLS growth and lateral expansion by vapor-solid (VS) edge incorporation produces a characteristic triangular shape (Figure 1 (e)). Hence, similar to the Ga-chalcogenides, the choice of chalcogen affects the selection between nanowires and ribbons.

Possible mechanisms governing the layer orientation include catalyst-substrate interactions at

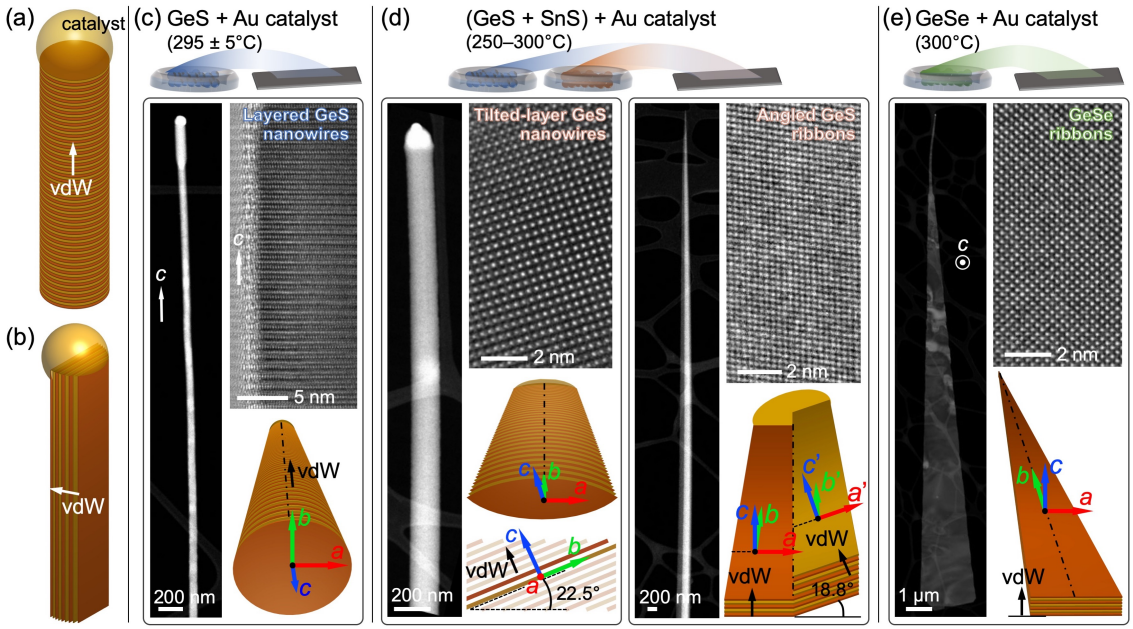

Figure 1. Towards control over the layer orientation. (a) VdW nanowire with layer stacking parallel to the growth direction. **(b)** Nanoribbon with stacking perpendicular to the growth direction. **(c)** Au-catalyzed VLS growth from a pure GeS precursor yields GeS nanowires with layer stacking along the growth direction (case (a)). **(d)** Adding small amounts of SnS to the GeS precursor switches the product to two new morphologies: Tilted-layer GeS nanowires with layering at 22.5° from the long axis (left); and angled GeS ribbons, whose joined halves intersect at 18.8° (right). In both cases, the added SnS acts only as a growth modifier without being incorporated significantly in the nanostructures. **(e)** Au-catalyzed VLS growth from a GeSe precursor yields large, ultrathin GeSe ribbons with layer stacking perpendicular to the growth direction (case (b)). Overview images: STEM. High-resolution images: TEM. (c), (d) Adapted with permission from ref. [2]. Copyright 2021 American Chemical Society. (e) adapted with permission from ref. [25]. Copyright 2021 Royal Society of Chemistry.

the initial growth stages and processes involving the wetting of the growth front by the molten catalyst. Advanced experiments (*e.g.*, *in-situ* microscopy during growth)[26-28] may allow identifying the primary mechanism(s) controlling the layer orientation. An alternative strategy, based on modifying the catalyst, furnished evidence for the key role of the VLS catalyst and its wetting of the growth front in selecting the layer orientation and provided access to layering between the limiting cases shown in Figure 1 (a)–(b). While Au-catalyzed growth of Ge-chalcogenides involves a Au-Ge(S, Se) quasi-binary catalyst, adding a Sn-chalcogenide (*e.g.*, SnS) to the precursor changes the catalyst to a Au-Ge-Sn(S, Se) quasi-ternary. An immediate effect is a significant opening of the temperature window for VLS synthesis, from (295 ± 5) °C

using pure GeS (below the growth temperature for Ge nanowires over Au-Ge catalyst due to a chalcogen-induced modification of the phase diagram)[1,13,29] to 250–300 °C with mixed (GeS, SnS).[30] Importantly, this change takes place already at low vapor pressures of the additive, where SnS acts as a growth modifier without being incorporated significantly in the nanostructures.[2]

GeS nanostructures obtained from mixed (GeS, SnS) vapors at 265 °C switch to two distinct morphologies: Tilted-layer nanowires and angled nanoribbons (Figure 1 (d)). Both types of nanostructures carry Au-rich VLS catalyst particles at their tips, but while the catalyst of nanowires obtained with pure GeS precursor (Figure 1 (c)) contains only Au, Ge, and S, EDS shows the presence of Sn in the catalyst of nanostructures obtained with (GeS, SnS). This change of the catalyst correlates with modifications to the morphology. Tilted-layer nanowires adopt a vdW layering at a shallow (22.5°) angle relative to the growth axis, intermediate between nanowires (90°) and ribbons (0°). Angled nanoribbons are asymmetric bicrystals whose two halves, joined at a central grain boundary, intersect at an angle of ~19°. Similar modifications to the layering were reported for a different materials system, namely Pb-catalyzed PbI_2 nanowires, where added $PbBr_2$ switched the layer orientation from $[0001]$ to $[2\bar{1}\bar{1}0]$ or induced $[\bar{2}021]$-axis twinning.[31]

3. DOMINANT (FAST-GROWING) DEFECT MORPHOLOGIES

VLS growth of 3D-crystalline semiconductor nanowires typically produces high-quality single crystals. Exceptions include III-V nanowires with stacking faults or zincblende-wurtzite polytype switching,[32] Ge nanowires formed by twin-plane reentrant growth,[33] as well as branched Pb-chalcogenide (PbSe,[34] PbS)[35] nanowires whose main branch is a growth spiral around an axial screw dislocation. The latter two cases – twin- and dislocation-assisted growth – are examples of processes in which materials incorporation at the growth front involves a

reduced or vanishing activation energy, so that the axial growth rate is enhanced compared to the defect-free case where adding each monolayer requires an activated nucleation event.

Recent work shows VLS growth of vdW nanostructures dominated by fast-growing/defect morphologies, some of which mirror those observed for 3D-crystals: *(i)* Nanoribbons, growing by incorporation from the catalyst into open edges of the layered crystal (Figure 2 (a));[2,23-25,36,37] *(ii)* chiral twisted nanowires formed by spiral growth around an axial screw dislocation (Figure 2 (b));[1,30,38,39] and *(iii)* bicrystals growing by a twin-plane reentrant process (Figure 2 (c)).[3,31] Compared with defect-free wires, such fast-growing nanostructures achieve a significantly greater length. Hence, the nanostructure selection during VLS growth follows an evolutionary process, where the system initially explores a large number of possible morphologies of which the fastest-growing ones collect most of the incoming vapor and become the predominant synthesis product.

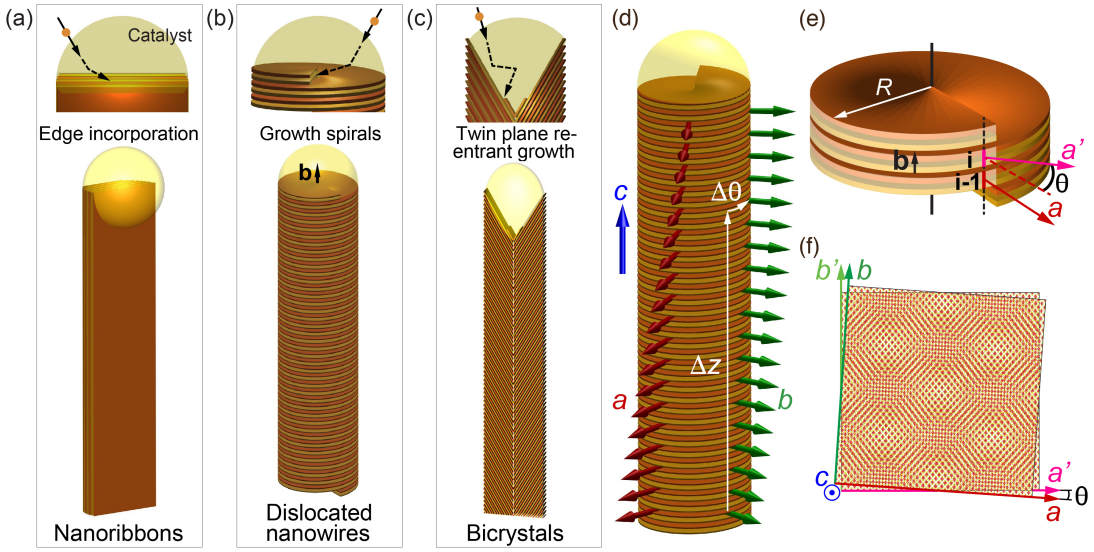

Figure 2. Fast-growing vdW nanostructures obtained by VLS growth. (a) Nanoribbons growing by incorporation from the catalyst into open layer edges. **(b)** Chiral twisted vdW nanowires, in which an axial screw dislocation enables nucleationless growth. **(c)** VdW bicrystals that grow by a twin-plane re-entrant process. **Eshelby twist and interlayer twist in van der Waals nanowires. (d)** Schematic of a chiral twisted vdW nanowire with progressive rotation of the in-plane (*a*, *b*) lattice vectors due to Eshelby twist. **(e)** Eshelby twist translates into small-angle interlayer twist between consecutive turns of the helical nanowires. **(f)** Twist moiré pattern projected onto the helicoid vdW interface. (e), (f) adapted with permission from ref. [38]. Copyright 2020 Wiley-VCH.

Dislocated GeS nanowires were obtained by VLS growth from a pure GeS precursor at typical substrate temperatures close to 300 °C, using Au[1,38] or Bi[39] catalysts. Under these conditions, a large majority (>95%) of the resulting nanowires incorporate axial screw dislocations, *i.e.*, adopt fast spiral growth. GeS bicrystal nanoribbons incorporating a central mirror twin boundary were obtained as a second fast-growing morphology by VLS growth over

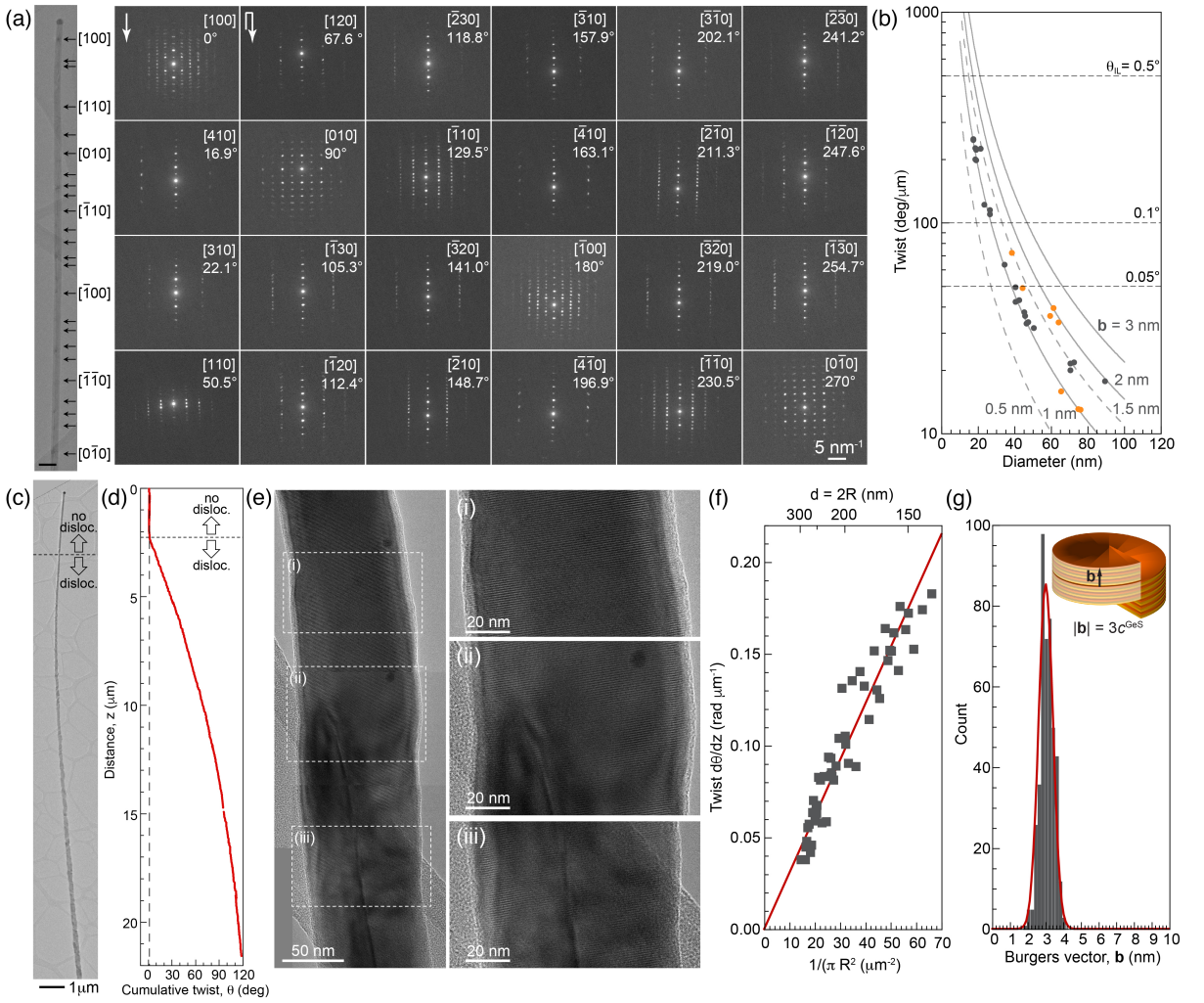

Figure 3. Chiral twisted vdW nanowires. (a) TEM image and nanobeam electron diffraction (NBD) of an ultrathin (18 nm) GeS nanowire obtained with Bi VLS catalyst, showing the progression between different electron-beam zone axes (arrows in image; labels in NBD patterns). **(b)** Eshelby twist in GeS vdW nanowires. Yellow and gray symbols: Au and Bi catalyst, respectively. θ_{IL}: Interlayer twist. **Twist homojunctions. (c)** TEM image of a GeS nanowire in which the screw dislocation is expelled ~2.2 μm from the tip. **(d)** Cumulative twist obtained from NBD along the wire. **(e)** High-resolution TEM of a GeS nanowire near the position where the dislocation is expelled. **Continuously varying Eshelby twist. (f)** Twist analysis along a tapered GeS nanowire, demonstrating continuously varying Eshelby twist. **(g)** Burgers vector analysis, showing **|b|** = 3 c^{GeS}. (a), (b) adapted with permission from ref. [39]. Copyright 2021 Wiley-VCH. (c)–(g) adapted with permission from ref. [38]. Copyright 2020 Wiley-VCH.

Bi catalysts at 300 °C.[3] Similar bicrystals were also synthesized at reduced temperatures of 245–300°C over Au catalysts using GeS as precursor and SnS as growth modifier.[3]

A powerful way of obtaining novel properties from 2D/layered materials involves stacking with a small interlayer twist. Effects arising from the resulting twist moirés include superconductivity,[40] moiré excitons,[41,42] ferroelectricity,[43] *etc*. To date, twisted vdW stacks have been realized primarily by top-down mechanical assembly.[44] In bottom-up vdW epitaxy, adjacent layers tend to lock into their (aligned) equilibrium registry,[45] and protocols allowing controllable interlayer twist are only beginning to be developed.[46,47] VLS growth of vdW nanowires with axial screw dislocations inherently provides stable, precisely tunable interlayer twist suitable for the emerging field of 3D twistronics.[48] The dislocation induces Eshelby twist,[49] where the dislocation stress-field exerts a torque between the ends of the nanowire, thus causing a progressive lattice rotation along the wire of magnitude per unit length $\mathrm{d}\theta/\mathrm{d}z = \boldsymbol{b}/[\pi R^2]$, where **b** denotes the Burgers vector of the screw component of the dislocation and πR^2 is the cross-sectional area of the nanowire (Figure 2 (d)). For a layered crystal, Eshelby twist translates into interlayer twist, *i.e.*, produces a twist moiré projected onto a helicoid vdW interface (Figure 2 (e)). In ultrathin nanowires with diameters below 20 nm, interlayer twists of ~0.3° have been realized (Figure 3 (a), (b)),[39] and angles of 1° or are feasible in even thinner wires or screw dislocations with larger Burgers vector. The twist angle is precisely tunable *via* the nanowire diameter (selected *via* the catalyst size), and the dislocation stabilizes the moiré against re-orientation to the aligned registry. Hence, twisted nanowires provide an alternative to mechanically stacked bilayers for accessing emergent electronic phenomena in group IV chalcogenides.[50]

Nanobeam electron diffraction (NBD) provides a convenient tool for quantifying Eshelby twist. Figure 3 (a) shows the twist analysis using a NBD linescan along an ultrathin GeS nanowire grown over Bi catalyst. The rotation of the in-plane (*a*, *b*) crystal axes is reflected in a continuous change of the zone axis along the wire, progressing from $[100]$ near the tip to $[0\bar{1}0]$ near the bottom of the field of view (270° cumulative twist over 1.34 μm length). A similar analysis for many wires with different diameters shows that the continuum Eshelby formalism holds down to the thinnest nanowires, and that GeS wires incorporate screw dislocations with Burgers vectors that are both integer and half-integer multiples of the GeS unit cell size, $c^{GeS} \approx 1$ nm. In the latter case, crystallography requires a non-equilibrium stacking of consecutive GeS layers, which is non-centrosymmetric and could cause ferroelectricity in dislocated GeS wires.[39]

Twisted vdW nanowires offer additional opportunities for creating exotic sample geometries. For example, twisted and aligned (layered) segments can be joined within single nanowires, if the screw dislocation is expelled during growth. An abrupt lowering of the sample temperature and resulting vacancy injection provide an edge component causing the dislocation to climb to the surface (Figure 3 (c)). In this way, Eshelby twist is terminated and the wire continues with ordinary vdW layering (Figure 3 (d), (e)). The realization of such twist homojunctions yields samples that are ideal for understanding twist-induced functionality by directly comparing measurements on twisted and layered parts of the same nanowire (see Section 4.).

A second advanced geometry is realized in tapered van der Waals nanowires whose diameter steadily increases from base to tip, due to combined axial VLS and lateral vapor-solid growth.[38] Such wires provide deeper insight into both Eshelby twist and helical twist moirés. As envisioned by Eshelby, the twisting of dislocated rods is indeed a differential property, *i.e.*, any two cross-sections of a rod containing an axial screw dislocation (separated by a distance d*z*)

experience a twist $d\theta = \boldsymbol{b}/[\pi R^2]\,\mathrm{d}z$. Analysis of NBD linescans along tapered dislocated GeS nanowires provides experimental confirmation of this concept (Figure 3 (f)), by demonstrating that each segment indeed incorporates a twist $\mathrm{d}\theta(z)$ that corresponds to the local cross-section $\pi R^2(z)$. Note that, as expected, the Burgers vector **b** of the screw dislocation remains constant along the entire nanowire ($3c^{\mathrm{GeS}}$ in Figure 3 (g)). In the context of the physics of twist moirés, these results have additional implications. Since the moiré pattern is projected onto a helicoid-

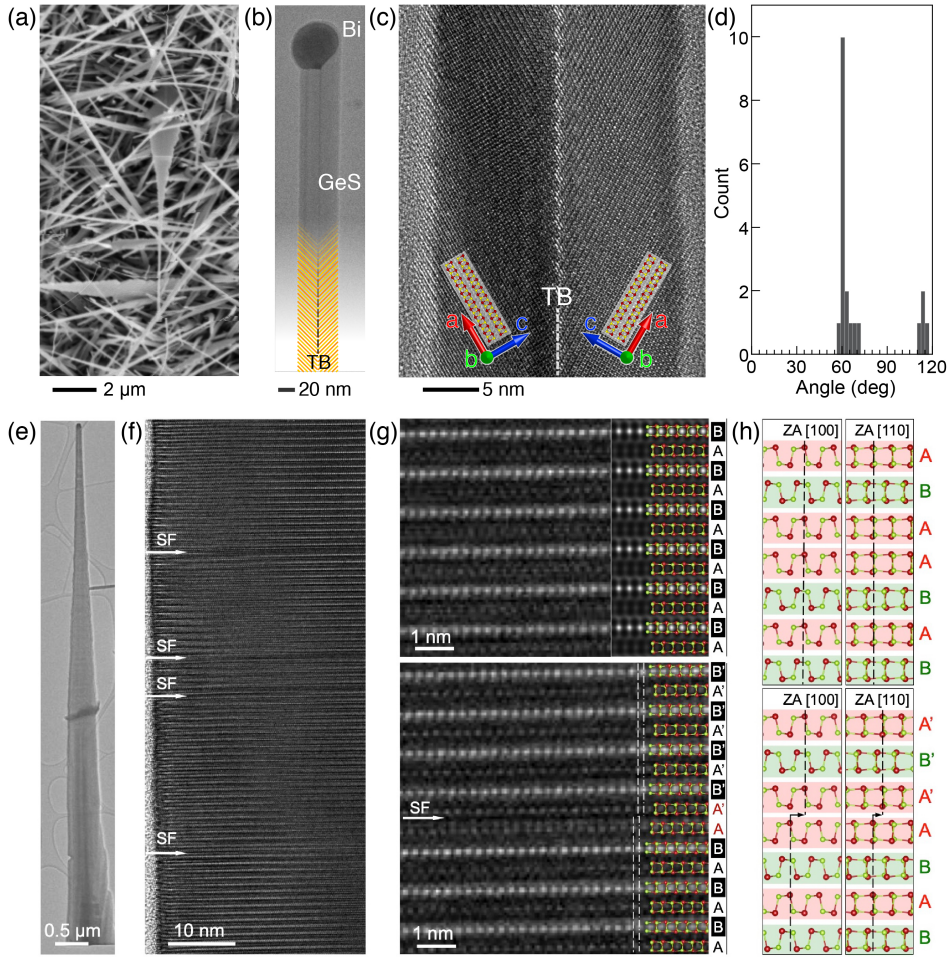

Figure 4. Other 1D vdW defect morphologies. Bicrystals. (a) SEM image of GeS bicrystals and nanowires obtained by Bi-catalyzed VLS growth. **(b)** TEM image of the straight tip section of a GeS bicrystal. **(c)** High-resolution TEM image showing the two halves separated by a twin boundary (TB). **(d)** Histogram of the angles between the (001) planes on either side of the twin. **Stacking faults in layered nanowires. (e)** TEM image of a $GeSe_{0.7}S_{0.3}$ alloy nanowire. **(f)** High-resolution TEM showing single-layer stacking faults (SF) embedded in the AB-stacked wire. **(g)** High-resolution TEM (zone axis [110]) of an AB-stacked segment (top) and region around a single-layer stacking fault (bottom). **(h)** Possible stacking orders, AA (top) and AA' (bottom), viewed along [100] and [110] zone axes (ZA). (a)–(d) adapted with permission from ref. [3]. Copyright 2022 American Chemical Society. (e)–(h) adapted with permission from ref. [4]. Copyright 2022 American Chemical Society.

shaped interface (see Figure 2 (e), (f)), the thickness-dependent twist along a tapered wire translates into a continuously varying interlayer twist (and moiré period) along the interface, an architecture that has no equivalent in the planar topology of conventional twisted vdW stacks.

In GeS vdW bicrystals (Figure 4 (a), (b)), a second prevalent defect morphology, the growth front is generally formed by (001) planes, mostly enclosing angles of 60° and symmetric over the entire length, suggesting that they formed simultaneously (Figure 4 (c)–(d)). During VLS growth, the liquid catalyst is expected to wet the two halves of the bicrystal symmetrically, positioned in the V-groove at the growth front. This geometry is analogous to twinned germanium nanowires, where two Ge (111) planes meet at the twin and the layer nucleation barrier is reduced by a negative line energy at the junction between the twin in the nucleus and the adjacent solid-liquid interfaces.[33] The observation of bicrystals as a fast-growing GeS morphology suggests that a similarly reduced nucleation barrier facilitates VLS growth of vdW bicrystals. While enabling fast growth, spectroscopy shows that the twin-plane defect in GeS bicrystals is surprisingly benign electronically, *i.e.*, does not cause non-radiative recombination (see Section 4.).

Finally, not all defect morphologies of 1D vdW nanostructures involve imperfections that promote fast growth, but they can harbor unusual functionality. For example, VLS growth of GeS_xSe_{1-x} alloys with $x < 0.6$ produces nanowires with layering along the growth axis (see Section 2.). Here, addition of each atomic layer requires nucleation and the resulting wires tend to be strongly tapered (Figure 4 (e)). In vdW crystals, such layer nucleation can select between different possible stacking arrangements. For group IV monochalcogenides, the equilibrium (AB) stacking involves alternating A- and B-layers and bulk crystals retain mirror symmetry.[51] Few-layer crystals with metastable AA stacking, on the other hand, were shown to be

ferroelectrics.[52] Calculations for GeS_xSe_{1-x} alloys show a decreasing stacking fault energy with increasing Se content,[4] *i.e.*, Se-rich alloys may spontaneously introduce layers with non-equilibrium stacking. High-resolution TEM of $GeSe_{0.7}S_{0.3}$ alloy nanowires indeed confirms the formation of frequent single-layer stacking faults (Figure 4 (f)). Analysis by high-resolution TEM (Figure 4 (g)) and STEM shows that the faulted layers are not AA-stacked but adopt a previously unknown AA'-stacking where the additional A-layer is shifted by half a unit cell along [010] (Figure 4 (h)). The local symmetry breaking due to such stacking faults promises emerging functionality such as ferroelectricity in vdW nanowires.

4. FUNCTIONALITY FROM DEFECTS: OPTOELECTRONICS, PHOTONICS, FERROELECTRICITY

Whereas planar twist moirés lend themselves to investigation by various scanning probe microscopies, such as scanning tunneling microscopy/spectroscopy,[53,54] piezoresponse force microscopy,[55] and scanning near-field optical microscopy,[56] accessing the (opto-) electronics of chiral twisted vdW nanowires and other 1D layered nanostructures poses additional challenges, *e.g.*, due to the small lateral size, the unusual topology of the helicoid interface carrying the twist moiré, *etc*. Correlated electron microscopy techniques can successfully address these challenges by providing information on crystal structure, optical absorption, and luminescence from the same nanometer-scale region within single vdW nanostructures (Figure 5 (a)). NBD uses a few-nm parallel electron beam to obtain local structure information, whereas the focused beam in STEM enables both nanoscale absorption (electron energy loss spectroscopy, EELS) and cathodoluminescence (STEM-CL) spectroscopies.

Figure 5 (b)–(d) illustrates the use of hyperspectral STEM-CL linescans for probing the moiré energy landscape along twisted GeS nanowires, whose twist angle has been determined by

NBD (Figure 3). The exciting electron beam is scanned along the wire and CL spectra are obtained at each point (Figure 5 (b)–(c)). Their analysis yields data such as the wavelength λ_0 of the dominant emission (Figure 5 (d)), which changes systematically due to the varying moiré registry along the wire with a bandgap variation $\Delta E_g \approx 240$ meV, consistent with moiré potential landscapes found in planar systems.[57]

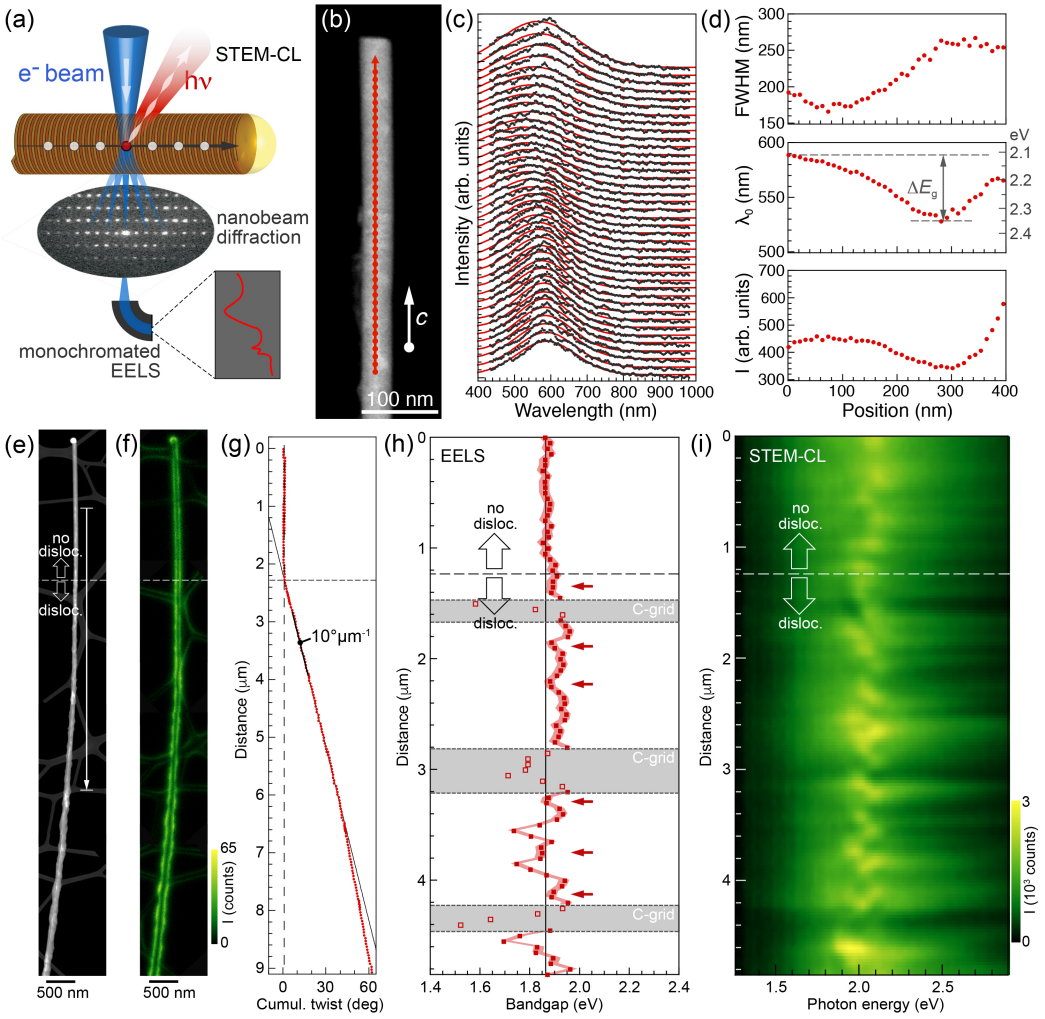

Figure 5. Nanometer-scale optoelectronic spectroscopy. (a) Correlated spectroscopies in STEM: Light emission (STEM-CL), optical absorption (EELS), and local structure (NBD). **Moiré registry-dependent bandgap in twisted vdW nanowires. (b)** STEM image of a twisted GeS nanowire. **(c)** STEM-CL spectra obtained at points marked in (b), with Gaussian fits (red). **(d)** Fit-analysis showing systematic changes in linewidth (FWHM), center wavelength (λ_0), and intensity (I) along the wire. **Correlated NBD, STEM-CL, and monochromated EELS. (e)** STEM image of a GeS nanowire containing a twist homojunction. **(f)** Panchromatic CL map of the wire. **(g)** Twist analysis of NBD patterns obtained along the nanowire. **(h)** EELS bandgap measurement along the nanowire (arrow in (e)). **(i)** Hyperspectral STEM-CL linescan along the same section of the nanowire. (b)–(d) adapted with permission from ref. [1]. Copyright 2019 Springer Nature. (e)–(i) adapted with permission from ref. [38]. Copyright 2021 Wiley-VCH.

Figure 5 (e)–(i) illustrates the power of correlated NBD, EELS, and CL measurements on tailored samples, such as nanowires containing twist junctions. Imaging (Figure 5 (e)) and NBD analysis (Figure 5 (g)) identify the location of the junction between the layered tip- and twisted base-regions of the wire. Monochromated EELS shows a constant bandgap in the non-dislocated tip region transitioning into large bandgap variations in the twisted portion of the wire. STEM-CL along the same wire demonstrates bright light emission (Figure 5 (f)) as well as luminescence properties mirroring those found in absorption (Figure 5 (i)), *i.e.*, pronounced swings in photon energy in the twisted part of the wire.

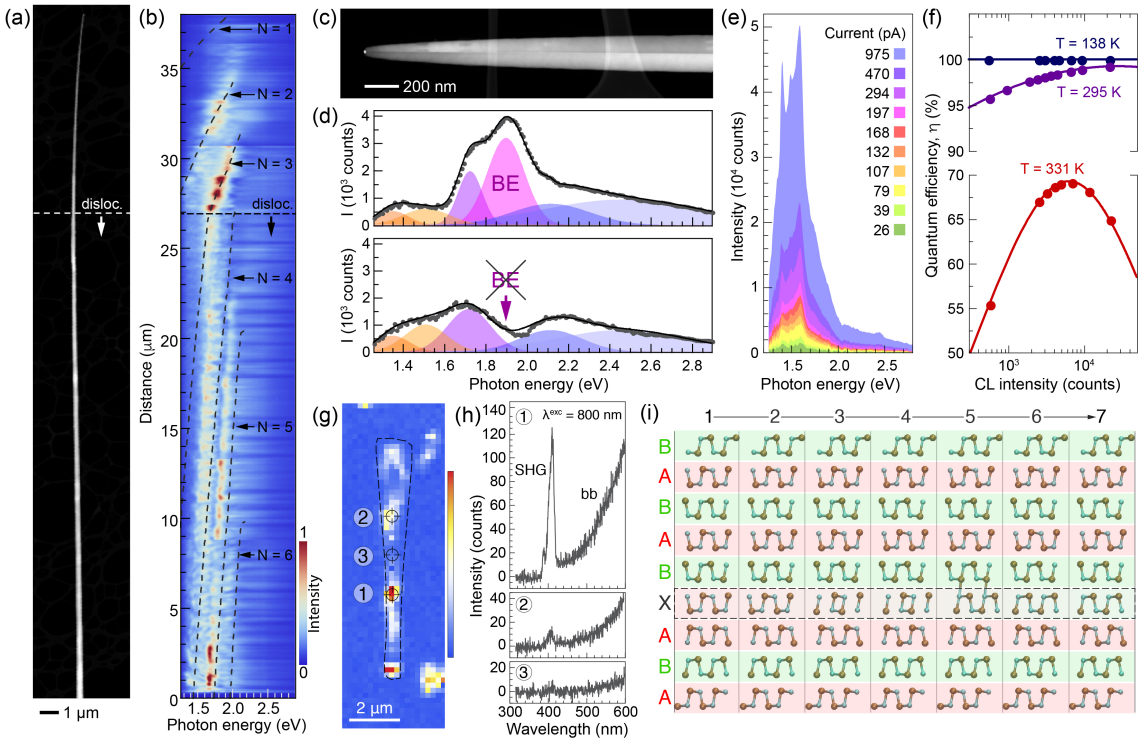

Figure 6. Photonics, optoelectronics, and ferroelectricity. Chiral whispering gallery modes (WGMs). (a) Thick tapered GeS nanowire with dislocated and defect-free segments joined at a twist junction. **(b)** Hyperspectral STEM-CL linescan showing a blue-shift due to chiral WGMs in the dislocated part of the wire. **Effect of defects on radiative recombination. (c)** GeS vdW bicrystal obtained with SnS-modified Au catalyst. **(d)** CL spectra unaffected (top) and modified (bottom) by non-radiative recombination at the twin boundary. **(e)** Electron beam-current dependent STEM-CL spectra measured on a GeS bicrystal at T = 138 K. **(f)** Analysis of beam-current dependent CL to obtain the spontaneous emission quantum efficiency. **Symmetry breaking by stacking faults. (g)** Second harmonic generation (SHG) map of a GeS_xSe_{1-x} nanowire. **(h)** Selected SHG spectra along the wire. **(i)** Pathway of polarization switching for a single-layer stacking fault. (a), (b) adapted with permission from ref. [30]. Copyright 2023 Royal Society of Chemistry. (c)–(f) adapted with permission from ref. [3]. Copyright 2022 American Chemical Society. (g)–(i) adapted with permission from ref. [4]. Copyright 2022 American Chemical Society.

Thicker GeS nanowires with twist junctions (Figure 6 (a)) allowed identifying chirality effects due to the helical structure caused by an axial screw dislocation, by comparing STEM-CL of whispering gallery photonic modes (WGMs) in dislocated and defect-free portions of the wires (bands of intense light emission in Figure 6 (b)). Whereas the modes observed in layered (defect-free) segments closely match with simulations, those in dislocated parts show a characteristic blue-shift assigned to chiral WGMs (Figure 6 (b)).[30]

STEM-CL can also probe the effects of defects on radiative recombination in vdW nanostructures.[3] Bicrystal ribbons grown over SnS-modified Au catalysts (Figure 6 (c)) predominantly show the emission characteristics of bulk GeS, blue-shifted due to confinement. Only in exceptional cases do CL spectra show the quenching of the band-edge luminescence due to the opening of a non-radiative recombination channel with short carrier lifetime, associated with mid-gap states (Figure 6 (d)). Electron beam-current dependent CL (Figure 6 (e)), analogous to power-dependent photoluminescence,[58] can be used to quantify the spontaneous emission quantum efficiency in single nanostructures. The measurements demonstrate unity or near-unity quantum efficiencies at low- and room temperature, respectively, thus highlighting the electronically benign nature of the twin defect in GeS bicrystal ribbons and raising the prospect of harnessing defects for the synthesis of vdW nanostructures without compromising their (opto-) electronic properties.

We conclude with an example of emerging functionality of vdW nanostructures beyond optoelectronics and photonics. As discussed in Section 3., VLS growth of Se-rich GeS_xSe_{1-x} alloys produces layered nanowires with AA' stacking faults inserted into the equilibrium (AB) stacked host (Figure 4). Symmetry breaking due to the stacking faults can be demonstrated experimentally by second-harmonic generation (SHG) spectroscopy. Hyperspectral maps show

alternating areas with high and low SHG signal (Figure 6 (h)–(i)), consistent with alternating stacking fault-rich regions and extended AB stacked areas in the GeS_xSe_{1-x} nanowires. The breaking of inversion symmetry by AA' stacking faults raises the prospect of ferroelectricity carried by such planar defects in vdW crystals. Indeed, *ab-initio* calculations identify a rational pathway for polarization switching in the inserted A'-layer, which behaves much like an isolated single-layer monochalcogenide ferroelectric[51] both in terms of its spontaneous polarization as well as the switching energy barrier. The strategy of incorporating layers carrying a spontaneous electric polarization establishes a class of ferroelectrics based on vdW nanostructures, beyond the known planar thin film ferroelectrics comprising either 3D- or 2D/layered crystals.

5. CONCLUSIONS AND OUTLOOK

As we discussed in this Account, 1D van der Waals nanostructures such as nanowires, nanoribbons, *etc.*, are a fascinating class of nanomaterials providing a rich playground for synthesis as well as promising functionality. In comparison to 3D-crystalline nanowires obtained by VLS growth, vdW nanostructures offer additional structural degrees of freedom such as a variable layer orientation, which due to the strong in-plane/cross-plane anisotropy will translate into tunable properties. Often, however, other factors prevail and simple layered structures are not formed in the growth process. Indeed, concerted research efforts during the past few years provided evidence for the propensity of vdW nanostructures to select specific defect morphologies that involve reduced or even vanishing layer nucleation barriers, show fast growth, and thus become the dominant synthesis product. Importantly, not only do the defects have little or no negative impact on key electronic effects such as radiative recombination and light emission, but they give access to unconventional properties including helical twist moirés and associated bandgap modulations, chiral photonics, and ferroelectricity originating from

symmetry breaking at single-layer defects.

Clearly, the field of 1D vdW nanostructures offers ample opportunities for future research. Open questions for the nanostructures discussed in this Account include the microscopic mechanisms governing the introduction of ubiquitous screw dislocations in GeS nanowires and their suppression by minor changes to the materials chemistry, *e.g.*, alloying of GeS with GeSe. An important research direction will be to expand the library of vdW materials from which nanowires and related nanostructures can be obtained, beyond the monochalcogenides that have been the focus of recent research. Findings for group IV monochalcogenides point to properties that may support VLS growth of 1D nanostructures from other layered materials. Examples of such properties include an enhanced surface reactivity (favoring layer nucleation) and strong interlayer interaction (key to maintaining planar layering) compared to most 2D/layered materials, along with a propensity toward spiral growth (supporting the introduction of screw dislocations).[59]

Prior work also demonstrated how competing growth pathways, such as the VLS process involving mass transport through a liquid catalyst and direct vapor-solid (VS) incorporation, can work in concert to shape the growing nanostructures.[25] Recent results suggest that differences between VLS and VS incorporation for different elements may additionally provide control over the composition. For example, differences in transport of Ge-sulfides and -selenides through Au catalysts were exploited to assemble mixed-dimensional $GeS_{1-x}Se_x$ alloy heterostructures joining 1D (VLS) nanowires and 2D (VS) plates with substantially different S:Se ratio.[60]

Going from single-component nanostructures to heterostructures incorporating different vdW crystals carries large potential for future discoveries. Recent examples illustrate that the results can be quite surprising, beyond the well-known band structure engineering through integration of

different electronic materials. Lattice mismatch in nanoribbon heterostructures, for instance, can induce axial twisting, *i.e.*, shaping into the 3rd dimension. This was realized by growth from mixed (GeS, SnS) precursors, which yields $Ge_{1-x}Sn_xS$ alloy ribbons whose edge is enriched with SnS. The larger lattice constant of the Sn-rich alloy causes compressive edge-stress,[61] inducing spontaneous axial twisting (Figure 7 (a)). STEM-CL combined with simulations (Figure 7 (b)–(c)) demonstrates the coherent excitation of propagating exciton-polariton modes by the electron beam in vertical sections, whereas only weak localized fields are induced in planar portions of the ribbons. Such 3D-shaped vdW ribbons are promising as waveguides for integrated photonic architectures. Core-shell vdW nanowires are at the heart of emerging approaches for generating single dislocations with tunable character, taking advantage of the reduced set of Burgers vectors in layered crystals.[62] In the presence of a screw dislocation, the *c*-axis lattice mismatch between

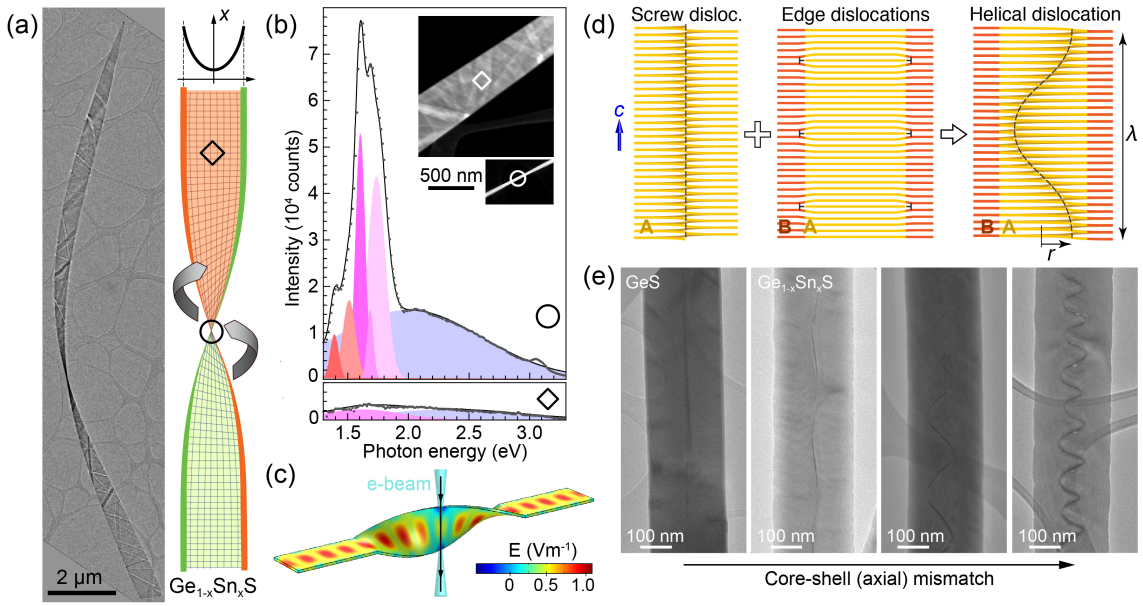

Figure 7. Future opportunities in 1D vdW heterostructures. 3D-shaped nanoribbons. (a) TEM image of a $Ge_{1-x}Sn_xS$ nanoribbon showing spontaneous axial twisting. **(b)** STEM-CL spectra obtained in planar and vertical sections of a twisted nanoribbon. **(c)** Simulation of the electron-beam excitation of a propagating polariton waveguide mode in the vertical ribbon section. **Dislocation mixing in core-shell vdW nanowires. (d)** Mixing of screw- and edge-dislocations to generate single helical dislocations with tunable screw/edge ratio. **(e)** Demonstration of dislocation mixing in $Ge_{1-x}Sn_xS$ core-shell nanowires. (a)–(c) adapted with permission from ref. [36]. Copyright 2021 Wiley-VCH. (d), (e) adapted with permission from ref. [62]. Copyright 2023 American Chemical Society.

core and shell, which would otherwise be relaxed *via* edge dislocations, converts the screw into a mixed (helical) dislocation with tunable ratio between screw- and edge Burgers vector components (Figure 7 (d)). Figure 7 (e) shows the realization of this concept using $Ge_{1-x}Sn_xS$ wires that spontaneously phase-separate into a GeS-rich core and SnS-enriched shell. $Ge_{1-x}Sn_xS$ alloy wires with increasing core-shell mismatch indeed progress from pure screw dislocations to mixed (helical) dislocations with predominant edge component. The ability to create single mixed dislocations with tunable character promises to enable the exploration of the emerging properties of quantized dislocations (dislons),[63] so that line defects can be harnessed in technological applications.

COMPETING INTERESTS. The authors declare no competing financial interest.

BIOGRAPHIES

Peter Sutter is Professor of Electrical and Computer Engineering at the University of Nebraska-Lincoln. He received M.S. and Ph.D. degrees in Physics from ETH Zürich. Following postdoctoral work at the University of Wisconsin-Madison, he held appointments as Assistant/Associate Professor in Physics at the Colorado School of Mines and Group Leader in the Center for Functional Nanomaterials at Brookhaven National Laboratory. His research focuses on 2D/layered materials and nanomaterials, studied by microscopy and nanometer-scale spectroscopy.

Eli Sutter is Professor of Mechanical and Materials Engineering at the University of Nebraska-Lincoln. She earned M.S. and Ph.D. degrees in Condensed Matter Physics from Sofia University "St. Kliment Ohridski", Bulgaria, followed by postdoctoral fellowships at ETH Zürich and at the University of Wisconsin-Madison, and appointments as Assistant Professor of Physics at the Colorado School of Mines and as Scientist in the Center for Functional Nanomaterials at Brookhaven National Laboratory. Her research focuses on transmission electron microscopy and spectroscopy of 2D/layered materials and nanomaterials.

ACKNOWLEDGEMENTS. This work was supported by the National Science Foundation, Division of Materials Research, Solid-State and Materials Chemistry Program under Grants No. DMR-1904843 and DMR-2315397.

REFERENCES

1. Sutter, P.; Wimer, S.; Sutter, E. Chiral twisted van der Waals nanowires. *Nature* **2019,** 570, 354-357.
2. Sutter, E.; French, J. S.; Sutter, P. Tunable Layer Orientation and Morphology in Vapor–Liquid–Solid Growth of One-Dimensional GeS van der Waals Nanostructures. *Chem. Mater.* **2021,** 33, 3980-3988.
3. Sutter, E.; French, J. S.; Komsa, H.-P.; Sutter, P. 1D Germanium Sulfide van der Waals Bicrystals by Vapor–Liquid–Solid Growth. *ACS Nano* **2022,** 16, 3735-3743.
4. Sutter, E.; Komsa, H.-P.; Puretzky, A. A.; Unocic, R. R.; Sutter, P. Stacking Fault Induced Symmetry Breaking in van der Waals Nanowires. *ACS Nano* **2022,** 16, 21199-21207.
5. Geim, A. K.; Novoselov, K. S. The rise of graphene. *Nat. Mater.* **2007,** 6, 183-191.
6. Manzeli, S.; Ovchinnikov, D.; Pasquier, D.; Yazyev, O. V.; Kis, A. 2D transition metal dichalcogenides. *Nat. Rev. Mater.* **2017,** 2, 17033.
7. Iijima, S. Helical microtubules of graphitic carbon. *Nature* **1991,** 354, 56-58.
8. Chopra, N. G.; Luyken, R. J.; Cherrey, K.; Crespi, V. H.; Cohen, M. L.; Louie, S. G.; Zettl, A. Boron Nitride Nanotubes. *Science* **1995,** 269, 966-967.
9. Tenne, R.; Margulis, L.; Genut, M.; Hodes, G. Polyhedral and cylindrical structures of tungsten disulphide. *Nature* **1992,** 360, 444-446.
10. Feldman, Y.; Wasserman, E.; Srolovitz, D. J.; Tenne, R. High-Rate, Gas-Phase Growth of MoS_2 Nested Inorganic Fullerenes and Nanotubes. *Science* **1995,** 267, 222-225.
11. Balandin, A. A.; Kargar, F.; Salguero, T. T.; Lake, R. K. One-dimensional van der Waals quantum materials. *Materials Today* **2022,** 55, 74-91.
12. Wagner, R. S.; Ellis, W. C. Vapor-Liquid-Solid Mechanism of Single Crystal Growth. *Appl. Phys. Lett.* **2004,** 4, 89-90.
13. Sutter, E.; Sutter, P. 1D Wires of 2D Layered Materials: Germanium Sulfide Nanowires as Efficient Light Emitters. *ACS Appl. Nano Mater.* **2018,** 1, 1042-1049.
14. Peng, H.; Meister, S.; Chan, C. K.; Zhang, X. F.; Cui, Y. Morphology Control of Layer-Structured Gallium Selenide Nanowires. *Nano Lett.* **2007,** 7, 199-203.
15. Vaughn, D., II; Sun, D.; Levin, S. M.; Biacchi, A. J.; Mayer, T. S.; Schaak, R. E. Colloidal Synthesis and Electrical Properties of GeSe Nanobelts. *Chem. Mater.* **2012,** 24, 3643-3649.
16. Zhai, T.; Fang, X.; Liao, M.; Xu, X.; Li, L.; Liu, B.; Koide, Y.; Ma, Y.; Yao, J.; Bando, Y.; Golberg, D. Fabrication of High-Quality In_2Se_3 Nanowire Arrays toward High-Performance Visible-Light Photodetectors. *ACS Nano* **2010,** 4, 1596-1602.
17. Yang, R. B.; Bachmann, J.; Pippel, E.; Berger, A.; Woltersdorf, J.; Gösele, U.; Nielsch, K. Pulsed Vapor-Liquid-Solid Growth of Antimony Selenide and Antimony Sulfide Nanowires. *Advanced Materials* **2009,** 21, 3170-3174.
18. Primak, W.; Fuchs, L. H. Electrical Conductivities of Natural Graphite Crystals. *Phys. Rev.* **1954,** 95, 22-30.
19. Slack, G. A. Anisotropic Thermal Conductivity of Pyrolytic Graphite. *Phys. Rev.* **1962,** 127, 694-701.

20. Krishnan, K. S.; Ganguli, N. Large Anisotropy of the Electrical Conductivity of Graphite. *Nature* **1939,** 144, 667-667.
21. Wu, Y.; Cui, Y.; Huynh, L.; Barrelet, C. J.; Bell, D. C.; Lieber, C. M. Controlled Growth and Structures of Molecular-Scale Silicon Nanowires. *Nano Lett.* **2004,** 4, 433-436.
22. Schmidt, V.; Senz, S.; Gösele, U. Diameter-Dependent Growth Direction of Epitaxial Silicon Nanowires. *Nano Lett.* **2005,** 5, 931-935.
23. Sutter, E.; French, J. S.; Sutter, S.; Idrobo, J. C.; Sutter, P. Vapor–Liquid–Solid Growth and Optoelectronics of Gallium Sulfide van der Waals Nanowires. *ACS Nano* **2020,** 14, 6117-6126.
24. Sutter, P.; French, J. S.; Khosravi Khorashad, L.; Argyropoulos, C.; Sutter, E. Optoelectronics and Nanophotonics of Vapor–Liquid–Solid Grown GaSe van der Waals Nanoribbons. *Nano Lett.* **2021,** 21, 4335-4342.
25. Sutter, E.; French, J. S.; Sutter, P. Free-standing large, ultrathin germanium selenide van der Waals ribbons by combined vapor–liquid–solid growth and edge attachment. *Nanoscale* **2022,** 14, 6195-6201.
26. Panciera, F.; Chou, Y. C.; Reuter, M. C.; Zakharov, D.; Stach, E. A.; Hofmann, S.; Ross, F. M. Synthesis of nanostructures in nanowires using sequential catalyst reactions. *Nat. Mater.* **2015,** 14, 820-825.
27. Maliakkal, C. B.; Jacobsson, D.; Tornberg, M.; Persson, A. R.; Johansson, J.; Wallenberg, R.; Dick, K. A. In situ analysis of catalyst composition during gold catalyzed GaAs nanowire growth. *Nat. Commun.* **2019,** 10, 4577.
28. Harmand, J.-C.; Patriarche, G.; Glas, F.; Panciera, F.; Florea, I.; Maurice, J.-L.; Travers, L.; Ollivier, Y. Atomic Step Flow on a Nanofacet. *Phys. Rev. Lett.* **2018,** 121, 166101.
29. Sutter, E. A.; Sutter, P. W. Size-Dependent Phase Diagram of Nanoscale Alloy Drops Used in Vapor−Liquid−Solid Growth of Semiconductor Nanowires. *ACS Nano* **2010,** 4, 4943-4947.
30. Sutter, P.; Khosravi-Khorashad, L.; Ciobanu, C. V.; Sutter, E. Chirality and dislocation effects in single nanostructures probed by whispering gallery modes. *Mater. Horiz.* **2023,** 10, 3830-3839
31. Huh, L.; Shim, H.; Shin, N. Br-Induced Orientation Control of PbI_2 van der Waals Nanowires and Their Optoelectronics. *ACS Photonics* **2021,** 8, 3291-3300.
32. Glas, F.; Harmand, J.-C.; Patriarche, G. Why Does Wurtzite Form in Nanowires of III-V Zinc Blende Semiconductors? *Phys. Rev. Lett.* **2007,** 99, 146101.
33. Gamalski, A. D.; Voorhees, P. W.; Ducati, C.; Sharma, R.; Hofmann, S. Twin Plane Re-entrant Mechanism for Catalytic Nanowire Growth. *Nano Lett.* **2014,** 14, 1288-1292.
34. Zhu, J.; Peng, H.; Marshall, A. F.; Barnett, D. M.; Nix, W. D.; Cui, Y. Formation of chiral branched nanowires by the Eshelby Twist. *Nat. Nanotechnol.* **2008,** 3, 477-481.
35. Bierman, M. J.; Lau, Y. K. A.; Kvit, A. V.; Schmitt, A. L.; Jin, S. Dislocation-Driven Nanowire Growth and Eshelby Twist. *Science* **2008,** 320, 1060-1063.
36. Sutter, P.; Khorashad, L. K.; Argyropoulos, C.; Sutter, E. Cathodoluminescence of Ultrathin Twisted $Ge_{1-x}Sn_xS$ van der Waals Nanoribbon Waveguides. *Adv. Mater.* **2021,** 33, 2006649.
37. Jung, C. S.; Park, K.; Shojaei, F.; Oh, J. Y.; Im, H. S.; Lee, J. A.; Jang, D. M.; Park, J.; Myoung, N.; Lee, C.-L.; Lee, J. W.; Song, J. K.; Kang, H. S. Photoluminescence and Photocurrents of $GaS_{1-x}Se_x$ Nanobelts. *Chem. Mater.* **2016,** 28, 5811-5820.
38. Sutter, P.; Idrobo, J.-C.; Sutter, E. Van der Waals Nanowires with Continuously Variable Interlayer Twist and Twist Homojunctions. *Adv. Funct. Mater.* **2021,** 31, 2006412.

39. Sutter, E.; Sutter, P. Ultrathin Twisted Germanium Sulfide van der Waals Nanowires by Bismuth Catalyzed Vapor–Liquid–Solid Growth. *Small* **2021,** 17, 2104784.
40. Cao, Y.; Fatemi, V.; Fang, S.; Watanabe, K.; Taniguchi, T.; Kaxiras, E.; Jarillo-Herrero, P. Unconventional superconductivity in magic-angle graphene superlattices. *Nature* **2018,** 556, 43-50.
41. Jin, C.; Regan, E. C.; Yan, A.; Iqbal Bakti Utama, M.; Wang, D.; Zhao, S.; Qin, Y.; Yang, S.; Zheng, Z.; Shi, S.; Watanabe, K.; Taniguchi, T.; Tongay, S.; Zettl, A.; Wang, F. Observation of moiré excitons in WSe_2/WS_2 heterostructure superlattices. *Nature* **2019,** 567, 76-80.
42. Tran, K.; Moody, G.; Wu, F.; Lu, X.; Choi, J.; Kim, K.; Rai, A.; Sanchez, D. A.; Quan, J.; Singh, A.; Embley, J.; Zepeda, A.; Campbell, M.; Autry, T.; Taniguchi, T.; Watanabe, K.; Lu, N.; Banerjee, S. K.; Silverman, K. L.; Kim, S.; Tutuc, E.; Yang, L.; MacDonald, A. H.; Li, X. Evidence for moiré excitons in van der Waals heterostructures. *Nature* **2019,** 567, 71-75.
43. Zheng, Z.; Ma, Q.; Bi, Z.; de la Barrera, S.; Liu, M.-H.; Mao, N.; Zhang, Y.; Kiper, N.; Watanabe, K.; Taniguchi, T.; Kong, J.; Tisdale, W. A.; Ashoori, R.; Gedik, N.; Fu, L.; Xu, S.-Y.; Jarillo-Herrero, P. Unconventional ferroelectricity in moiré heterostructures. *Nature* **2020,** 588, 71-76.
44. Kim, K.; Yankowitz, M.; Fallahazad, B.; Kang, S.; Movva, H. C. P.; Huang, S.; Larentis, S.; Corbet, C. M.; Taniguchi, T.; Watanabe, K.; Banerjee, S. K.; LeRoy, B. J.; Tutuc, E. van der Waals Heterostructures with High Accuracy Rotational Alignment. *Nano Lett.* **2016,** 16, 1989-1995.
45. Woods, C. R.; Withers, F.; Zhu, M. J.; Cao, Y.; Yu, G.; Kozikov, A.; Ben Shalom, M.; Morozov, S. V.; van Wijk, M. M.; Fasolino, A.; Katsnelson, M. I.; Watanabe, K.; Taniguchi, T.; Geim, A. K.; Mishchenko, A.; Novoselov, K. S. Macroscopic self-reorientation of interacting two-dimensional crystals. *Nat. Commun.* **2016,** 7, 10800.
46. Zhao, Y.; Zhang, C.; Kohler, D. D.; Scheeler, J. M.; Wright, J. C.; Voyles, P. M.; Jin, S. Supertwisted spirals of layered materials enabled by growth on non-Euclidean surfaces. *Science* **2020,** 370, 442-445.
47. Sutter, P.; Ibragimova, R.; Komsa, H.-P.; Parkinson, B. A.; Sutter, E. Self-organized twist-heterostructures via aligned van der Waals epitaxy and solid-state transformations. *Nat. Commun.* **2019,** 10, 5528.
48. Wu, F.; Zhang, R.-X.; Das Sarma, S. Three-dimensional topological twistronics. *Phys. Rev. Research* **2020,** 2, 022010.
49. Eshelby, J. D. Screw Dislocations in Thin Rods. *J. Appl. Phys.* **1953,** 24, 176-179.
50. Kennes, D. M.; Xian, L.; Claassen, M.; Rubio, A. One-dimensional flat bands in twisted bilayer germanium selenide. *Nat. Commun.* **2020,** 11, 1124.
51. Fei, R.; Kang, W.; Yang, L. Ferroelectricity and Phase Transitions in Monolayer Group-IV Monochalcogenides. *Phys. Rev. Lett.* **2016,** 117, 097601.
52. Higashitarumizu, N.; Kawamoto, H.; Lee, C.-J.; Lin, B.-H.; Chu, F.-H.; Yonemori, I.; Nishimura, T.; Wakabayashi, K.; Chang, W.-H.; Nagashio, K. Purely in-plane ferroelectricity in monolayer SnS at room temperature. *Nat. Commun.* **2020,** 11, 2428.
53. Zhang, Z.; Wang, Y.; Watanabe, K.; Taniguchi, T.; Ueno, K.; Tutuc, E.; LeRoy, B. J. Flat bands in twisted bilayer transition metal dichalcogenides. *Nat. Phys.* **2020,** 16, 1093-1096.
54. Xie, Y.; Lian, B.; Jäck, B.; Liu, X.; Chiu, C.-L.; Watanabe, K.; Taniguchi, T.; Bernevig, B. A.; Yazdani, A. Spectroscopic signatures of many-body correlations in magic-angle twisted bilayer graphene. *Nature* **2019,** 572, 101-105.

55. McGilly, L. J.; Kerelsky, A.; Finney, N. R.; Shapovalov, K.; Shih, E.-M.; Ghiotto, A.; Zeng, Y.; Moore, S. L.; Wu, W.; Bai, Y.; Watanabe, K.; Taniguchi, T.; Stengel, M.; Zhou, L.; Hone, J.; Zhu, X.; Basov, D. N.; Dean, C.; Dreyer, C. E.; Pasupathy, A. N. Visualization of moiré superlattices. *Nat. Nanotechnol.* **2020,** 15, 580-584.
56. Sunku, S. S.; Ni, G. X.; Jiang, B. Y.; Yoo, H.; Sternbach, A.; McLeod, A. S.; Stauber, T.; Xiong, L.; Taniguchi, T.; Watanabe, K.; Kim, P.; Fogler, M. M.; Basov, D. N. Photonic crystals for nano-light in moiré graphene superlattices. *Science* **2018,** 362, 1153-1156.
57. Shabani, S.; Halbertal, D.; Wu, W.; Chen, M.; Liu, S.; Hone, J.; Yao, W.; Basov, D. N.; Zhu, X.; Pasupathy, A. N. Deep moiré potentials in twisted transition metal dichalcogenide bilayers. *Nat. Phys.* **2021,** 17, 720-725.
58. Johnson, S. R.; Ding, D.; Wang, J.-B.; Yu, S.-Q.; Zhang, Y.-H. Excitation dependent photoluminescence measurements of the nonradiative lifetime and quantum efficiency in GaAs. *J. Vac. Soc. Technol. B* **2007,** 25, 1077-1082.
59. Sutter, P.; Sutter, E. Growth Mechanisms of Anisotropic Layered Group IV Chalcogenides on van der Waals Substrates for Energy Conversion Applications. *ACS Appl. Nano Mater.* **2018,** 1, 3026-3034.
60. Sutter, E.; Sutter, P. Self-Assembly of Mixed-Dimensional $GeS_{1-x}Se_x$ (1D Nanowire)–(2D Plate) Van der Waals Heterostructures. *Small* **2023,** DOI: 10.1002/smll.202302592.
61. Ramasubramaniam, A.; Koskinen, P.; Kit, O. O.; Shenoy, V. B. Edge-stress-induced spontaneous twisting of graphene nanoribbons. *J. Appl. Phys.* **2012,** 111, 054302.
62. Sutter, P.; Unocic, R. R.; Sutter, E. Deterministic Tuning of Single Mixed (Helical) Dislocations in Core-Shell van der Waals Nanowires. *J. Am. Chem. Soc.* **2023,** 145, 20503–20510.
63. Li, M. Quantized dislocations. *J. Phys. Condens. Matter* **2019,** 31, 083001.

CONSPECTUS GRAPHIC